Ligand Exchange Reactions in the Formation of Diphosphine-Protected Gold Clusters

ARTICLE *in* THE JOURNAL OF PHYSICAL CHEMISTRY C · AUGUST 2008

Impact Factor: 4.77 · DOI: 10.1021/jp804046e

Ligand Exchange Reactions in the Formation of Diphosphine-Protected Gold Clusters

Denis E. Bergeron,*,† Orkid Coskuner,*,†,‡ Jeffrey W. Hudgens,† and Carlos A. Gonzalez†

National Institute of Standards and Technology, 100 Bureau Drive, Stop 8380, Gaithersburg, Maryland 20899, Computational Materials Science Center, George Mason University, Research I, Fairfax, Virginia 22030

Received: May 7, 2008; Revised Manuscript Received: June 6, 2008

Ligand exchange reactions important in the formation of L^3- and L^5-protected gold clusters (L^3 = 1,3-bis(diphenylphosphino)propane; L^5 = 1,5-bis(diphenylphosphino)pentane) are investigated at the molecular level. We establish that molecular complexes, $[Au(PPh_3)_xL^n_{2-x}]^+$, in which Au^+ is bound to at least one triphenylphosphine ligand (PPh_3) act as precursors to cluster formation, while complexes in which Au^+ is bound only to the diphosphine ligands do not. Ligand exchange reactions and ion equilibria were studied via electrospray ionization mass spectrometry, and a critical reaction was studied with ab initio molecular dynamics simulations. The displacement of one PPh_3 by L^3 on $[Au(PPh_3)_2]^+$ was studied with transition path sampling calculations with Car−Parrinello molecular dynamics simulations. The experiments and simulations are in excellent agreement, and we demonstrate the applicability of these tools to chemical reactions involving ligand exchange.

I. Introduction

The thorough mechanistic description of formation reactions is a logical first step toward the realization of a rational synthetic approach to tailored nanoparticles. The general understanding of formation mechanisms for monolayer protected nanoparticles is that labile ligands alternately protect and expose the core, so that growth proceeds in a stepwise fashion until a kinetically and/or thermodynamically favored size is reached, at which point the ligands cease to be labile, so that the core is no longer exposed and, therefore, does not grow.[1,2] This general description is very useful for understanding the basics of particle formation, but it is phenomenological. Molecular-level descriptions of the formation process are necessary if truly tailored synthetic strategies are to be realized. Recently, electrospray ionization mass spectrometry (ESI-MS) has emerged as a promising technique for illuminating reaction mechanisms involving solution phase complexes and nanoparticles.[3–7] ESI-MS often yields data that complements nuclear magnetic resonance (NMR) or X-ray crystallography (XRC) data. ESI-MS techniques offer specific advantages in cases where the identification of complexes that are labile on the NMR time scale is desired or in cases where the complexes of interest are more soluble (less amenable to crystallization) than coexisting components of an analyte solution.[5,6]

Herein, we identify the inorganic complexes that play a critical role in the formation of diphosphine-protected gold clusters. Such monolayer protected gold clusters (MPCs) have been the subject of numerous reviews[1,2,8–12] and remain an extremely active area of research due to potential applications in electronics, catalysis, waste treatment, and medicine. The experiments described clearly identify specific ions as precursors to cluster formation and others that, once formed, impede cluster formation. We thus establish important details of a formation mechanism involving sequential ligand replacement reactions. In this paper, we address the initial ligand exchange reactions on the molecular complexes.

The experimental studies are complemented by ab initio molecular dynamics simulations, using the transition path sampling (TPS) method to treat rare bond breakage and formation events. Simulations of ligand exchange reactions are challenging due to the multiplicity of timescales involved in the reaction. It is crucial to employ specific sampling techniques to select and even generate ligand exchange configurations from an equilibrated sample. The TPS technique employed in this work has demonstrated success treating rare events such as water dissociation around metal ions, water autoionization, and protein folding.[13–15] Detailed reviews of the technique can be found in the literature.[16–18] Recent computational studies have reported that classical simulations predict different structural properties for biomolecules and biometallic complexes than ab initio molecular dynamics simulations.[19,20] In order to achieve the level of accuracy afforded by ab initio molecular dynamics simulations of bond breakage and formation,[13,14,19,21] we use Car−Parrinello molecular dynamics (CPMD) simulations coupled with TPS to investigate an organometallic ligand exchange mechanism.

We approach the reaction mechanism experimentally and computationally to converge on a consistent result. Our ESI-MS experiments establish the importance of specific ligand exchange reactions to the formation of nanoparticles, and we present evidence for preferred mechanisms. Our CPMD/TPS simulations are focused on the same mechanism accessed experimentally, so that we achieve cooperative experimental and computational inquiry.

II. Methods

A. Experiment. The MPCs were synthesized as described previously, and their mass spectra were consistent with previous observations.[3,22] Briefly, $AuClPPh_3$ (99.9+ %), L^3 or L^5 (L^3 = 1,3-bis(diphenylphosphino)propane, 97%; L^5 = 1,5-bis(diphenylphosphino)pentane, 97%), and borane tert-butylamine complex (the reducing agent, 97%) were dissolved in a 1:1:5 ratio in either chloroform or 1:1 methanol:chloroform. The reaction solutions were covered to minimize evaporative losses and

* To whom correspondence should be addressed.
† National Institute of Standards and Technology.
‡ George Mason University.

10.1021/jp804046e CCC: $40.75
Published on Web 07/25/2008

SCHEME 1: Ligand Exchange on Complexes Leading to Cluster Formation

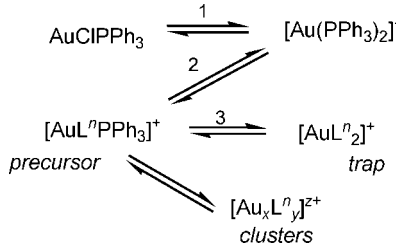

stirred. All chemicals and solvents were from Sigma Aldrich[23] and were used as delivered. As the reactions progressed in chloroform, aliquots were collected and diluted in methanol for ESI-MS analysis. In timed experiments, samples were analyzed within a few minutes (<5 min) of their dilution. Using the same procedure, the equilibria in chloroform of molecular complexes formed by L^n ligand exchange were also studied. During these experiments, L^3 or L^5 was added incrementally to a chloroform solution that contained $AuClPPh_3$ but no reducing agent, and samples were extracted from solution and analyzed by ESI-MS directly (i.e., in 100% chloroform).

Mass spectrometric measurements were performed with a dual probe electrospray ion source, including an integrated three vacuum stage and ion optics assembly (Analytica of Branford), coupled to a custom-built (by Ardara Technologies) Extrel CMS quadrupole mass spectrometer. Samples were introduced to the ESI source via direct infusion (10 μL/min), and the source was purged with ≥1.0 mL of methanol between each sample. Source conditions were optimized to maximize ion intensities while minimizing fragmentation. Monitoring the isotopic spacings at $[Au_xL_x^n]^{x+}$ ($x = 1$ or 2) gave some indication of the amount of fragmentation occurring; while $[Au_2L_2]^{2+}$ occurs in solution,[5,22] $[AuL]^+$ is a common fragment of the clusters we are studying.[22] The potential difference between the capillary exit and the skimmer was typically set to 80 V and samples in neat and diluted chloroform were observed to produce relatively stable ion currents.

B. Molecular Dynamics. To study rare events, such as bond breakage and formation, we applied the TPS method, using deterministic dynamics, to ligand exchange reaction 2 in Scheme 1. The TPS method is based on the generation of a set of transition pathways linking stable states of a physical system in phase space in a manner so that the first stable state (reactant) corresponds to $[Au(PPh_3)_2]^+$, where the PPh_3 ligand is coordinated to the Au ion. In the second state (product), the PPh_3 is replaced by L^3. These stable states are minima on the potential energy surface. Each path used in this study connects these two stable states in configurational space. A time step of the path that crosses the saddle points in the potential energy surface is the time step associated with the transition state (TS) of the ligand exchange reaction. In this study, transition paths were approximated by a Au−P (coordinated P) distance descriptor (reaction coordinate). Once two stable states are located, TPS works by generating a set of transition pathways, starting from a given initial trajectory (discussed below) using the shooting and shifting algorithm.[13,17] The momentum $\vec{p}_i$ of each particle is modified by $\delta\vec{p}_i$ and the integration of the equations of motion backward and forward yield a new trajectory. Trajectories connecting the two defined states (reactant and product) are accepted, and outliers are rejected according to Monte Carlo rules.[17] In a shifting move, a trajectory is obtained by deleting a segment of length δt from the forward move or from the backward move of an existing path. New trajectories of length δt are grown using the deterministic dynamics technique described in ref 17. After we set the transition path, the search for the time step associated with the TS is carried out using the probability criterion:[17] a configuration $(\vec{r}(t_{TS}), \vec{p}(t_{TS}))$ of a path is considered to represent the TS at time t_{TS} with trial configurations starting at t_{TS} and having a probability of 1/2 to reach each of the two stable states (reactants and products). Here we limited our study to 30 trial paths per time step due to the relatively large size of the molecule and large CPU time associated with ab initio simulations.[24]

The CPMD simulations were performed with the NWCHEM program.[25] The valence electronic structure was treated by density functional theory (DFT) using the Perdew-Burke-Ernzerhof generalized gradient approximation (PBE/GGA) with a double-ζ basis set and Troullier-Martin pseudopotentials[26] and a cutoff value of 140 Ry. The time step for the simulation was set to 0.1 fs, and the isotopic mass of deuterium was used to describe the hydrogen motions. Long-range electrostatic interactions were treated with the Ewald mesh method.[27] The combination of CPMD and TPS simulations was accomplished by selecting the time slice from an existing path and changing the corresponding momentum according to the rules described above and in refs 13 and 14. The modified phase space point was supplied to the simulation program. The CPMD program integrated the equations of motion and the Lagrangian of Car and Parrinello for $\delta t/\Delta t$ was used to produce the trajectories after the forward shot was determined by momentum rescaling. We then proceeded with the backward part of the shooting move as described above. A detailed summary of this algorithm with CPMD can be found in the literature.[13,14,17]

Using our recent implementation of well-known classical mechanical free energy methods with ab initio molecular dynamics simulations,[12,18–20] we applied the perturbation method of calculating the Gibbs free energy changes (ΔG) for the ligand exchange reaction whereby one PPh_3 is replaced by L^3 on $[Au(PPh_3)_2]^+$ (reaction 2, scheme 1), utilizing the trajectories obtained from CPMD simulations with TPS. The energy change between two states i and $i + 1$ with the Hamiltonians H_i and H_{i+1} was calculated via equation 1.[25]

$$\Delta G(\lambda_{i+1} - \lambda_i) = -kT \ln\langle \exp[-(H_{\lambda_{i+1}} - H_\lambda)/kT] \rangle_{\lambda i} \quad (1)$$

where λ is a coupling parameter with values $\lambda = 0$ and 1 representing the initial and final states, respectively (see refs 13 and 21 for details).

III. Results and Discussion

Our endeavors to elucidate the molecular details of MPC formation (Figure 1) led us to conclude that molecular complexes played an important role (vide infra). A firm understanding of the ion equilibrium without reducing agent is therefore critical to identifying displacement from the equilibrium during cluster formation.

A. Ligand Exchange Equilibria among Molecular Complexes. Figure 2 shows the fractional intensity of ions volatilized from a solution of $AuClPPh_3$ in chloroform to which increasing amounts of L^3 were added.[28] For each $[L^3]/[Au(PPh_3)_2]^+$ ratio, we established that the solution was at equilibrium by measuring ESI-MS spectra of solution samples over time until constant peak intensity ratios were observed. At long times, we observed increasing ligand oxidation but no change to the underlying equilibrium of the variously coordinated complexes. Figure 2 presents the ESI-MS ion intensity data as a fraction of the total ion current, so that at each $[L^3]/[Au(PPh_3)_2]^+$ ratio, the ions are represented in proportion to their relative concentrations in

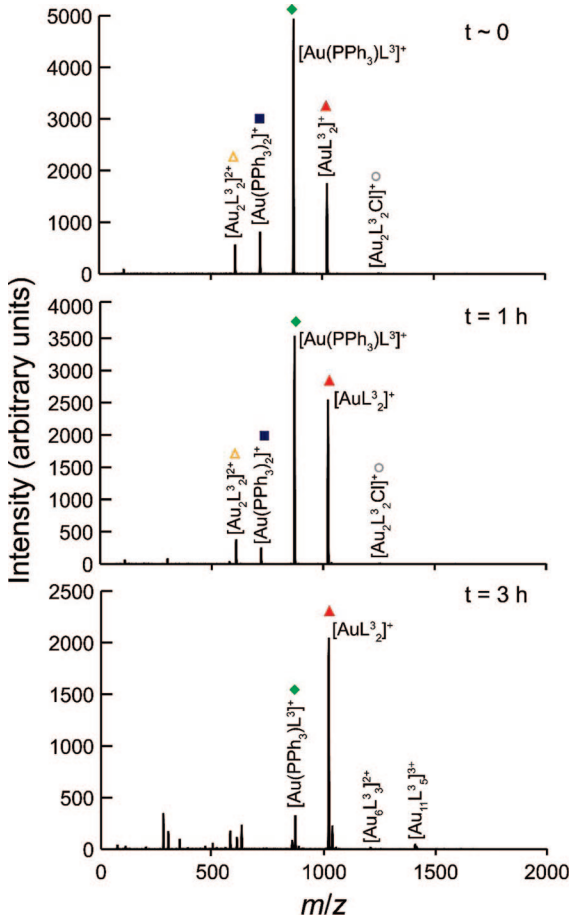

Figure 1. Mass spectra at three reaction times observed in the ESI-MS of a chloroform solution in which L^3-protected gold clusters are forming. After 3 h, the $[Au_{11}L^3_5]^{3+}$ cluster is present, and $[AuL^3_2]^+$ is the prominent molecular complex (see text). The symbols above the major peaks correspond to the symbol labels employed in Figure 2.

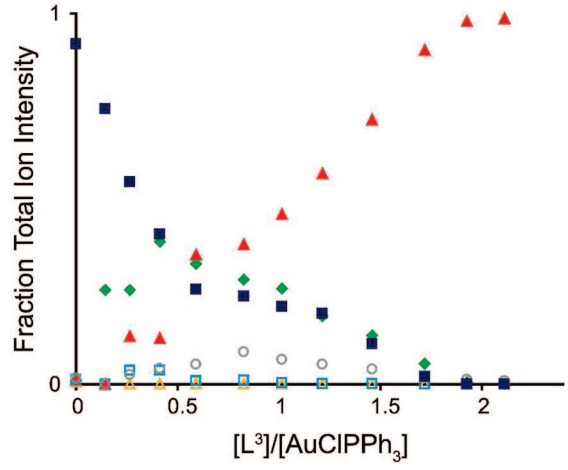

Figure 2. Fractional total ion current measured via ESI-MS as a function of the ratio $[L^3]/[AuClPPh_3]$. As L^3 was added gradually to $AuClPPh_3$ dissolved in chloroform, PPh_3 ligands are sequentially replaced on the Au^+ or Au_2^+ cores. The symbols are assigned as follows: solid blue square, $[Au(PPh_3)_2]^+$; solid green diamond, $[AuPPh_3L^3]^+$; solid red triangle, $[AuL^3_2]^+$; open orange triangle, $[Au_xL_x]^{x+}$; open blue square, $[Au_2PPh_3L^3Cl]^+$; open gray circle, $[Au_2L^3_2Cl]^+$. See text for details.

the solution, assuming that these ions are volatilized with essentially equal efficiencies.[29,30] Because the analytes share similar functional groups, we do not expect any complications[31] to arise from disparate ESI efficiencies.

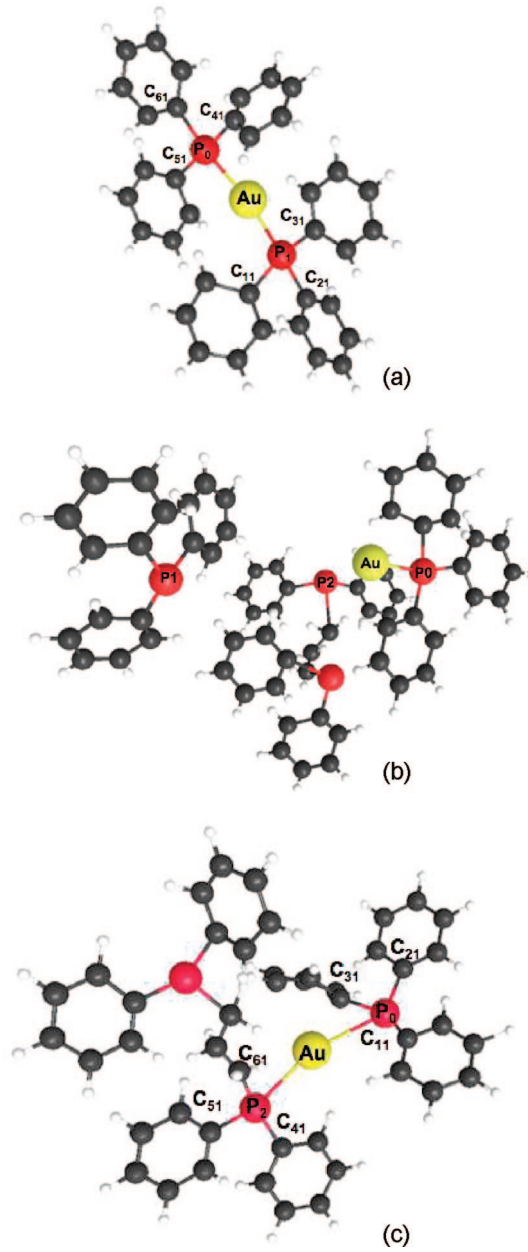

Figure 3. Equilibrium structures for (a) $[Au(PPh_3)_2]^+$ and (c) $[AuPPh_3L^3]^+$ determined via separate 40 ps CPMD simulations performed on initial structures obtained from CPMD/TPS simulations. The structure for the transition state (b) between these two complexes is also portrayed. Yellow represents gold, red phosphorus, black carbon, and white hydrogen.

According to Figure 2, L^3 readily replaces PPh_3 on $[Au(PPh_3)_2]^+$. As the L^3 concentration in the chloroform solution increases, the fractional abundance of $[Au(PPh_3)_2]^+$ steadily decays,[32] the fractional abundance of $[AuPPh_3L^3]^+$ increases to a maximum and then decays, and the fractional abundance of $[AuL^3_2]^+$ continuously increases. These data strongly support a sequential replacement reaction, as depicted in Scheme 1. Figure 2 also reveals that the addition of L^3 leads to the formation of digold complexes. This observation underscores the importance of reaction 2 of Scheme 1 in the promotion of cluster formation.

Figure 3 shows the reactant and product complexes for reaction 2 in Scheme 1. The equilibrium structure obtained for $[Au(PPh_3)_2]^+$ from our CPMD simulations indicates that the metal ion is asymmetrically coordinated to the two PPh_3 ligands

TABLE 1: Specific Average Bond Lengths and Angles for the $[Au(PPh_3)_2]^+$ Complex from CPMD Simulations, Shown in Figure 3a, and from experiment[a]

	CPMD simulations	experiment
Au−P1/Å	2.263 ± 0.110	2.321
Au−P0/Å	2.259 ± 0.130	2.322
P0−Au−P1/degrees	169.9 ± 4.3	167.3
P1−C11	1.86 ± 0.04	1.800
P1−C21	1.88 ± 0.05	1.823
P1−C31	1.83 ± 0.04	1.787
P0−C41	1.78 ± 0.06	1.801
P0−C51	1.84 ± 0.03	1.815
P0−C61	1.82 ± 0.03	1.789
P0−Au−P1	169.9 ± 4.3	167.3
Au−P1−C11	116.3 ± 2.9	112.7
Au−P1−C21	112.1 ± 2.3	107.8
Au−P1−C31	115.9 ± 3.2	119.3
Au−P0−C41	117.6 ± 2.6	114.8
Au−P0−C51	110.4 ± 3.0	107.5
Au−P0−C61	115.8 ± 3.5	117.4
C11−P1−C21	107.4 ± 1.4	105.2
C21−P1−C31	104.2 ± 1.8	105.6
C11−P1−C31	104.5 ± 1.1	105.2
C41−P1−C51	106.9 ± 0.8	104.8
C51−P0−C61	103.9 ± 1.5	106.9
C41−P0−C61	106.6 ± 0.9	104.5

[a] The computational results are in excellent agreement with crystallographic data from ref 33. All ± values refer to observed deviations from the equilibrium value, and not to uncertainties.

and that the $Ph_3P-Au-PPh_3$ angle is not linear (Table 1), possibly due to steric interactions. Overall, these structural results are consistent with the crystallographic data obtained by Wang (see Table 1 for details),[33] indicating that the structural parameters for crystalline $[Au(PPh_3)_2]^+$ differ by 2−11% from the gas phase values.

In addition, our CPMD simulations at 300 K indicate that there is a large (68.7 kJ/mol) potential energy barrier to ligand exchange. TPS is a viable method for investigating processes separated by high energy barriers,[14] and a 40 ps simulation, initiated from the 400 K trajectory, showed that $r(Au-P_1)$ (see Figure 3 for labeling) becomes >3.5 Å for $t = 1680$ fs. At this point, L^3 is beginning to displace PPh_3. In subsequent simulations, $r(Au-P_2)$ becomes <4.5 Å and $r(Au-P_0)$ increases from 2.4 Å to 2.9 Å. The distance $r(Au-P_2)$ becomes <3.7 Å for $t = 2910$ fs. Once the PPh_3 leaves the coordination shell (defined in this work as $r(Au-P_1) > 5$ Å), convergence to the equilibrium $[AuPPh_3L^3]^+$ structure occurs at $t = 3760$ fs, and for the remainder of the simulations, the average $r(Au-P_2)$ was found to be 2.8 Å with an average $r(Au-P_0)$ of 3 Å. At the end of our simulations, L^3 was 12% closer to Au^+ than PPh_3, reflecting that L^3 is a stronger Lewis base. No immediate return path leading to the formation of $[Au(PPh_3)_2]^+$ was observed on the time scale of our simulations. The PPh_3 ligand undergoes conformational changes when a L^3 ligand coordinates to the metal ion according to CPMD/TPS simulations performed on $[Au(PPh_3)_2]^+$ and $[AuPPh_3L^3]^+$.

The asymmetric binding of the ligands to the metal ion (see above) becomes more significant with the coordination of the L^3 ligand, with an average P_0-Au-P_2 angle of 133.7° ± 21.2° (where the ± value corresponds to observed deviations from the equilibrium value and does not represent an uncertainty) and presents a more floppy complex due to the ease of torsion about the bonds of the propyl chain. Table 2 lists the structural parameters obtained from separate 30 ps CPMD simulations for this complex. According to our simulations, the average

TABLE 2: Specific Average Bond Lengths and Angles for the $[AuPPh_3L^3]^+$ Complex Shown in Figure 2c[a]

Au−P0/Å	2.96 ± 0.39	Au−P2	2.77 ± 0.31
P0−C11	1.89 ± 0.05	P0−C21	1.91 ± 0.04
P0−C31	1.87 ± 0.02	P0−C41	1.88 ± 0.03
P2−C51	1.89 ± 0.04	P2−C61	1.86 ± 0.05
P0−Au−P2	133.7 ± 21.2	Au−P0−C11	104.9 ± 5.9
Au−P0−C21	119.1 ± 4.3	Au−P0−C31	107.7 ± 4.8
Au−P2−C41	118.6 ± 4.8	Au−P2−C51	120.1 ± 5.2
Au−P2−C61	112.3 ± 5.5	C11−P0−C21	105.3 ± 4.3
C21−P0−C31	101.0 ± 2.6	C11−P0−C31	107.9 ± 3.9
C41−P2−C51	107.6 ± 2.7	C51−P2−C61	108.5 ± 9.2
C41−P2−C61	110.4 ± 6.9		

[a] All ± values refer to observed (thermal) deviations from the equilibrium value, and not to uncertainties.

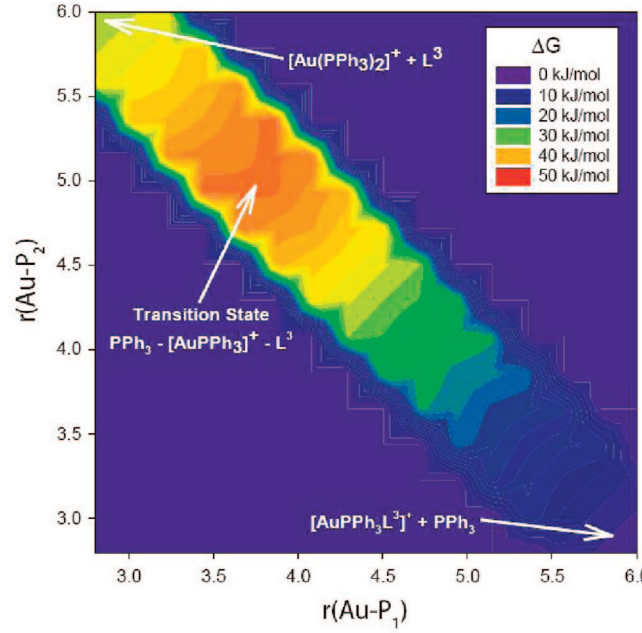

Figure 4. Calculated free energy change for the coordination of PPh_3 and L^3 on Au at 300 K. The transition pathway begins in the upper left corner with $[Au(PPh_3)_2]^+ + L^3$, and ends in the bottom right corner with $[AuPPh_3L^3]^+ + PPh_3$. The purple background is an artifact of the plotting program, and is not meant to imply that $\Delta G = 0$ outside of the diagonal of the transition path. See Figure 3 for the relevant structures and the text for further details.

Au−P distances for the coordinated P atoms of the two ligands increase by about 11−13% compared to the Au−P distances computed for the $[Au(PPh_3)_2]^+$ complex. Furthermore, the propyl chain carbon atoms of the L^3 ligand lead to more flexible $C-P_2-C$ angles compared to the angles involving ring C atoms (Tables 1 and 2).

According to the free energy change calculations (see Methods section for details), the coordination of L^3 to Au is ~30 kJ mol^{-1} more favorable than coordination of PPh_3 to Au, and a minimum is achieved with $r(Au-P_1) = 2.8$ Å (see Figure 3). The predicted Gibbs free energy change (Figure 4) shows a maximum when $r(Au-P_2) = 5.0$ Å and $r(Au-P_1) = 3.8$ Å. This is assigned as the transition state of the ligand exchange process. The Gibbs free energy of activation at 300 K ($\Delta G^{\#}$) is 46.2 kJ mol^{-1} (relative to the reactants). According to canonical transition state theory, the rate constant, k_{ex}, can be expressed

$$k_{ex} = \kappa \frac{k_B T}{h} \exp\left(-\frac{\Delta G^{\#}}{RT}\right) \quad (2)$$

where k_B is Boltzman's constant, T is the temperature, h is Planck's constant, R is the ideal gas constant, and κ (the

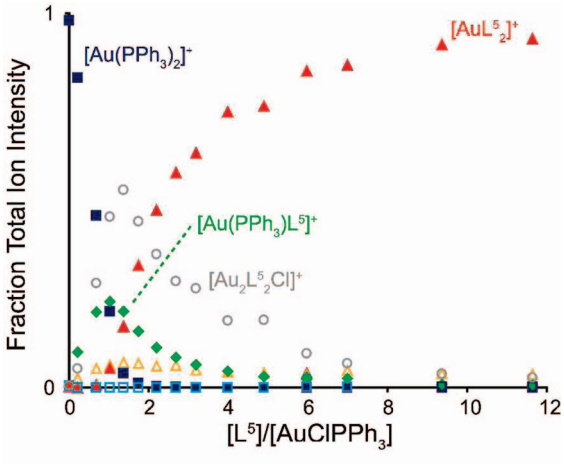

Figure 5. Fractional total ion current measured via ESI-MS as a function of the ratio $[L^5]/[AuClPPh_3]$. As L^5 was added gradually to $AuClPPh_3$ dissolved in chloroform, PPh_3 ligands are sequentially replaced on the Au^+ or Au_2^+ cores. The symbols are assigned as follows: solid blue square, $[Au(PPh_3)_2]^+$; solid green diamond, $[AuPPh_3L^5]^+$; solid red triangle, $[AuL^5_2]^+$; open orange triangle, $[Au_xL^5_x]^{x+}$; open blue square, $[Au_2PPh_3L^5Cl]^+$; open circle, $[Au_2L^5_2Cl]^+$.

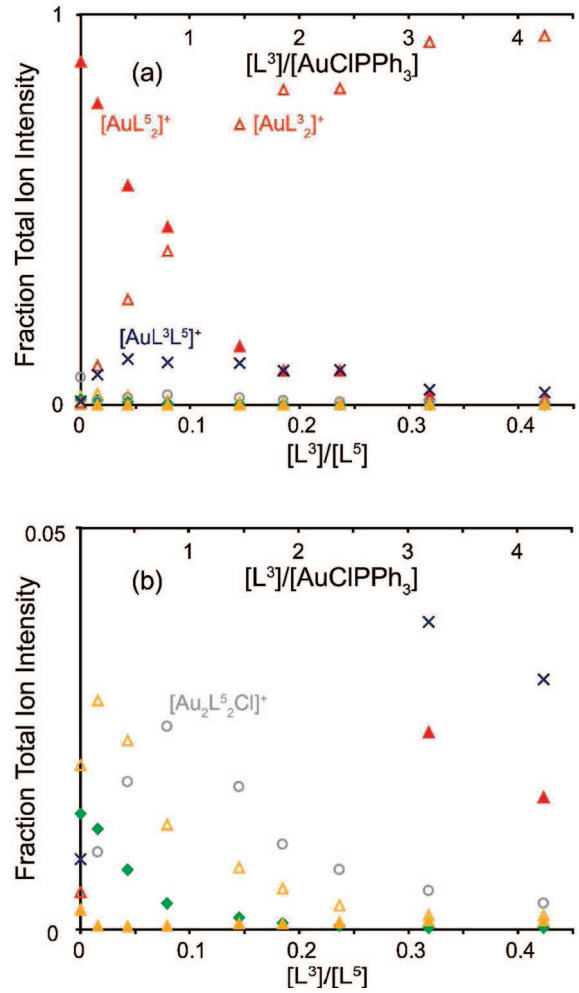

Figure 6. Fractional total ion current measured via ESI-MS as a function of $[L^3]/[L^5]$ (lower x-axis) and $[L^3]/[AuClPPh_3]$ (upper x axis). (a) As L^3 was added gradually to a solution containing Au:L^5 complexes, L^5 ligands are sequentially replaced. (b) A 20× magnification of (a). The diminishing contribution from Au_2^+ cores with increasing L^3 concentration indicates that they are broken into Au^+ cores due to the excess of ligand in the solution. The symbols are assigned as follows: solid red triangle, $[AuL^5_2]^+$; open orange triangle, $[Au_xL^5_x]^{x+}$; open blue square, $[Au_2PPh_3L^5Cl]^+$; open circle, $[Au_2L^5_2Cl]^+$; open red triangle, $[AuL^3_2]^+$; solid orange triangle, $[Au_xL^3_x]^{x+}$; × $[AuL^3L^5]^+$.

transmission coefficient) accounts for nonvibrational factors, such as tunneling and diffusion that contribute to passage through the transition state, and in many cases is found to be about unity.[34] For our reaction, we derive a k_{ex} value at 300 K of $5.6 \times 10^4\ s^{-1}$ if κ is assumed to be unity. We are encouraged that our predicted value falls in a range consistent with similar ligand exchange rates reported in the literature.[35]

The experimental determination of a rate constant can be achieved using the ratio I/I_0 (where, for example, I is the peak intensity of the $[Au(PPh_3)_2]^+$ reactant ion at a specific time or L^3 concentration and I_0 is the initial $[Au(PPh_3)_2]^+$ peak intensity), and so it is possible in principle to derive quantitative kinetics from these experiments despite the intrinsic uncertainties[31] of the ESI technique. Unfortunately, in the present case, difficulties in establishing reasonable initial intensities (I_0 values) arise due to the process whereby $AuClPPh_3$ forms the observable reactant, $[Au(PPh_3)_2]^+$ (reaction 1, Scheme 1).[32] Our data is, however, in good qualitative agreement with the results of the simulation and can reveal important aspects of the equilibria in question. Returning to Figure 2, it is clear that the first ligand replacement event, which we have simulated with CPMD/TPS, proceeds at relatively low concentrations of L^3, so that the proportion of $[Au(PPh_3)_2]^+$ and $[AuPPh_3L^3]^+$ is approximately equal even for $[L^3]/[AuClPPh_3] < 0.5$. Proceeding to higher L^3 concentrations, the appearance and disappearance of the $[Au(PPh_3)L^3]^+$ complex in Figure 2 indicates that the complete ligand replacement reaction proceeds in a sequential fashion, as shown in Scheme 1.

Experiments involving L^5 are depicted in Figures 5 and 6. The reaction mechanisms observed with L^5 mirror those found for L^3, but specific differences emerge in an analysis of the relevant equilibria. For example, comparing Figure 2 with Figure 5 shows that L^3 is more efficient than L^5 at replacing PPh_3. The reaction follows the same sequential replacement mechanism (Scheme 1) as for L^3, but when L^5 is involved, the ratio $[L^5]/[AuClPPh_3]$ must be much larger to achieve the same final equilibrium distribution of ions. The major difference between the reactions with L^3 and with L^5 is the behavior of the Au_2 complexes. In particular, for the L^3 reactions, the $[Au_2L^3_2Cl]^+$ complex appears as a minor constituent of the solution (Figure 2), peaking at $[L^3]/[AuClPPh_3] \approx 0.8$. In contrast, for the L^5 reactions, $[Au_2L^5_2Cl]^+$ is prominent up to relatively high (≈ 1.2) $[L^5]/[AuClPPh_3]$ ratios (Figure 5). In both cases, the initial replacement of PPh_3 by L^n according to

$$[Au_2PPh_3L^nCl]^+ + L^n \rightleftharpoons [Au_2L_2{}^nCl]^+ + PPh_3 \qquad (3)$$

is followed by

$$[Au_2L_2{}^nCl]^+ + L^n \rightleftharpoons [AuL_2{}^n]^+ + AuL^nCl \qquad (4)$$

Furthermore, by adding L^3 to a solution of Au:L^5 complexes, we produced Figure 6, which demonstrates that L^3 can readily displace L^5:

$$[AuL_2{}^5]^+ + L^3 \rightleftharpoons [AuL^3L^5]^+ + L^5 \qquad (5)$$

$$[AuL^3L^5]^+ + L^3 \rightleftharpoons [AuL_2{}^3]^+ + L^5 \qquad (6)$$

At $[L^3]/[AuClPPh_3] = 2$, L^5 is almost completely displaced, despite the fact that $[L^3]/[L^5]$ is only 1/5. L^5 is replaced by L^3 on the Au_2 complexes as well, and it appears that L^3 is more

efficient at breaking the Au−Au bond (as in eq 4) than L^5. These observations indicate that the bond between Au and L^3 is stronger than that between Au and L^5. It has been established that the length of the hydrocarbon chain between the two P atoms determines the preferred cluster size,[3,22] and it is possible that the relative preferences for mono- or digold complexes is similarly related to the length of the chain and its effect on the orientational angles.

B. Cluster Formation Reactions. Figure 1 shows a series of mass spectra collected via direct infusion of a chloroform solution in which L^3-protected gold clusters are forming. At very early times, contributions from the molecular complexes dominate the mass distribution. $[Au(PPh_3)_2]^+$, $[Au(PPh_3)L^3]^+$, and $[AuL^3_2]^+$ are joined by $[Au_2L^3_2]^{2+}$ and $[Au_2L^3_2Cl]^+$ to define the ion ensemble in the solution prior to substantial reduction. As the reaction proceeds, replacement of PPh_3 by L^3 is evident, and after 3 h, when the $[Au_{11}L^3_5]^{3+}$ cluster product is detected at 1409 *m/z*, significant $[AuL^3_2]^+$ is present, while the PPh_3-containing complexes are depleted. The disappearance of PPh_3-containing complexes in favor of $[AuL^n_2]^+$ is a general feature of the cluster formation reactions for both L^3 and L^5-protected clusters synthesized in either pure chloroform or 1:1 methanol: chloroform.

The formation of L^n-protected gold clusters from $AuClPPh_3$ requires two fundamental processes: growth of cluster cores and displacement of Cl and PPh_3 by L^n. The two processes are intimately intertwined because the cluster core cannot grow unless it is first exposed (or "deprotected"). Ligand removal events are therefore of profound importance in defining the kinetics and energetics of cluster formation. Scheme 1 illustrates this point in that the removal of one L^n ligand from $[AuL^n_2]^+$ (reverse reaction 3, Scheme 1) necessarily precedes cluster growth from $[AuL^n_2]^+$.

Scheme 1 is derived from our mass spectrometric data. Cluster syntheses are carried out with $[L^3]/[PPh_3] = 1$. At these concentrations, Figure 2 indicates that a significant contribution from each of the $[Au(PPh_3)_xL^3_{2-x}]^+$ ($x = 0-2$) complexes should be expected. At early times, Figure 1 indeed features peaks corresponding to $[Au(PPh_3)_2]^+$, $[AuPPh_3L^3]^+$, and $[AuL^3_2]^+$. However, as the reaction proceeds, the spectra favor $x = 0$ ($[AuL^3_2]^+$). In the absence of reducing agent, Figure 2 shows that x approaches 0 when $[L^3]/[PPh_3]$ increases. During the cluster synthesis, however, there is no change in $[L^3]/[PPh_3]$. These results indicate that the $x = 1$ and 2 complexes are reacting to contribute to cluster formation, while the $x = 0$ complex persists in solution. Hence, our mass spectrometric studies identify $[AuL^n_2]^+$ as a trap in the cluster formation reaction. It seems that the Au^+ core interacts much more strongly with L^n, and so it is not accessible as a nucleus for further growth which proceeds only when the reverse of reaction 3 from Scheme 1 occurs. Because $[AuL^n_2]^+$ is very stable, it forms readily, consuming much of the reactants. Once trapping has occurred, ligand removal (the reverse of reaction 3, Scheme 1) dictates cluster formation.

Even as the formation of the L^n-protected clusters results in an increasing proportion of PPh_3 in the solution, the displacement of L^n by PPh_3 only proceeds over the course of months, and we have found that throughout the course of our investigations (>6 months), $[AuL^n_2]^+$ complexes persist in solutions of clusters synthesized in 1:1 methanol:chloroform. Only a few other (larger) intermediates are observed in the reaction solutions, indicating that most reaction steps proceed on a much faster time scale than our multimonth survey is capable of resolving.

The trend, $L^3 > L^5 > PPh_3$, in the relative strengths of the interactions between Au^+ and each of our ligands is established. This definite trend is clearly important to a description of cluster formation. Several factors may contribute to the observed trend, including Lewis basicity, sterics, and potential bidentate coordination. We suspect that bidentate coordination is unimportant for monogold complexes (becoming important for digold and higher nuclearity species). Colton et al. reached a similar conclusion,[5] and our simulations also support an assertion that L^3 is monodentate in the complexes considered herein. Because mono- and bidentate coordination cannot be distinguished via mass spectrometry, we suggest that this issue might be resolved by detailed ^{31}P NMR investigations of the molecular complexes. However, in terms of the cluster formation reactions, it is more important that the diphosphine ligands are more strongly bound than PPh_3, and less important whether this is because of mono- v. bidentate coordination or because of sterics and electronics. Complexes (and clusters) in which Au is bound to Cl or PPh_3 are more likely to serve as reaction precursors than corresponding species in which Au is bound only to L^n because the more weakly interacting ligands are more labile, exposing the Au core to allow growth.

V. Conclusions

We employed ESI-MS and CPMD/TPS to describe the chemical processes involved in diphosphine-protected gold cluster formation. Our data provide significant insights regarding the mechanisms and equilibria involving ionic gold phosphine complexes, but the role of neutrals cannot be established in the present ESI-MS experiments. While the full complexity of the reaction solutions that we discuss is therefore inaccessible to our experimental approach, the detailed characterization of the ionic components should provide a sample of the rich chemistry at work. Furthermore, since the MPC products of interest are ionic species, it is reasonable to assume that the critical aspects of their formation can be established by following the ionic precursors. We identified specific precursor ions and discussed the importance of ligand lability in the cluster formation process. We showed evidence that $[AuL^n_2]^+$ represents a trap in the cluster formation reactions, as further growth requires the dissociation of L^n ligands (Scheme 1). Finally, we have employed ab initio molecular dynamics simulations with special sampling techniques to complement ESI-MS experiments and give a more complete picture of the chemical events, including bond breakage and formation, important to nanoparticle formation.

Together, our experiments and simulations addressed a critical ligand exchange reaction: ESI-MS provides the molecular details of the reaction, while CPMD/TPS provides the mechanistic details. The simulations are in accord with the experimental data, and reveal important thermodynamic and kinetic properties for the complexes and reactions involved in an early step of nanoparticle formation. The experimental and computational approach described herein promises to advance our understanding of diverse organometallic and biometallic problems ranging from the chemistry of nanomaterials to the mediation of protein secondary structure by metal ions.

Acknowledgment. We thank the NIST Center for Computational and Theoretical Nanoscience. D.E.B. acknowledges the National Academy of Science's National Research Council for a postdoctoral fellowship. We thank T. Allison (NIST) and D. Chandler (Berkeley) for helpful discussions.

Supporting Information Available: Figure S1 presents the ESI-MS data of Figure 2 as a function of ion signal intensity,

which is not normalized by the total ion current. This material is available free of charge via the Internet at http://pubs.acs.org.

References and Notes

(1) Daniel, M. C.; Astruc, D. *Chem. Rev.* **2004**, *104*, 293.
(2) Templeton, A. C.; Wuelfing, M. P.; Murray, R. W. *Acc. Chem. Res.* **2000**, *33*, 27.
(3) Bertino, M. F.; Sun, Z. M.; Zhang, R.; Wang, L. S. *J. Phys. Chem. B* **2006**, *110*, 21416.
(4) Tracy, J. B. C., M.C.; Parker, J. F.; Hampe, O.; Fields-Zinna, C. A.; Dass, A.; Murray, R. W. *J. Am. Chem. Soc.* **2007**, *129*, 16209.
(5) Colton, R.; Harrison, K. L.; Mah, Y. A.; Traeger, J. C. *Inorg. Chim. Acta* **1995**, *231*, 65.
(6) Traeger, J. C. *Int. J. Mass Spectrom.* **2000**, *200*, 387.
(7) Tracy, J. B.; Kalyuzhny, G.; Crowe, M. C.; Balasubramanian, R.; Choi, J. P.; Murray, R. W. *J. Am. Chem. Soc.* **2007**, *129*, 6706.
(8) Mingos, D. M. P.; Slee, T.; Lin, Z. Y. *Chem. Rev.* **1990**, *90*, 383.
(9) Schmid, G.; Corain, B. *Eur. J. Inorg. Chem.* **2003**, 3081.
(10) Pyykko, P. *Angew. Chem.-Int. Ed.* **2004**, *43*, 4412.
(11) Pyykko, P. *Inorg. Chim. Acta* **2005**, *358*, 4113.
(12) Pyykko, P. private communication, 2008.
(13) Coskuner, O.; Jarvis, E. A. A.; Allison, T. C. *Angew. Chem.-Int. Ed.* **2007**, *46*, 7853.
(14) Geissler, P. L.; Dellago, C.; Chandler, D.; Hutter, J.; Parrinello, M. *Science* **2001**, *291*, 2121.
(15) Bolhuis, P. G. *Proc. Natl. Acad. Sci. U.S.A.* **2003**, *100*, 12129.
(16) Dellago, C.; Bolhuis, P. G.; Csajka, F. S.; Chandler, D. *J. Chem. Phys.* **1998**, *108*, 1964.
(17) Bolhuis, P. G.; Chandler, D.; Dellago, C.; Geissler, P. L. *Annu. Rev. Phys. Chem.* **2002**, *53*, 291.
(18) Bolhuis, P. G.; Dellago, C.; Chandler, D. *Faraday Discuss.* **1998**, 421.
(19) Coskuner, O. *J. Chem. Phys.* **2007**, *127*, 015101.
(20) Coskuner, O.; Bergeron, D. E.; Rincon, L.; Hudgens, J. W.; Gonzalez, C. A. *J. Phys. Chem. A* **2008**, *112*, 2940.
(21) Coskuner, O.; Jarvis, E. A. A. *J. Phys. Chem. A* **2008**, *112*, 2628.
(22) Bergeron, D. E.; Hudgens, J. W. *J. Phys. Chem. C* **2007**, *111*, 8195.
(23) Certain commercial equipment, instruments, or materials are identified in this paper to foster understanding. Such identification does not imply recommendation or endorsement by the National Institute of Standards and Technology, nor does it imply that the materials or equipment identified are necessarily the best available for the purpose.
(24) Collection of the pathways used in this study took more than four months on a 25-node Sun Microsystems (Sun Fire 6800) cluster.
(25) Bylaska, E. J. d., W. A.; Kowalski, K.; et al. NWCHEM, A Computational Chemistry Package for Parallel Computers; 5.0 ed.; Pacific Northwest National Laboratory: Richland, WA, 2006.
(26) Troullier, N.; Martins, J. L. *Phys. Rev. B* **1991**, *43*, 1993.
(27) Allen, M. P.; Tildesley, D. J. *Computer Simulation of Liquids*; Clarendon Press/Oxford University Press: Oxford, 1987.
(28) Standard deviations for the data in Figures 2, 5, and 6 were examined. In most cases, we found $s < 1\%$. Maximal standard devations were found at intermediate concentration ratios; in all cases, we found $s < 10\%$. These deviations did not in any way obscure the overall trends.
(29) Cech, N. B.; Enke, C. G. *Mass Spectrom. Rev.* **2001**, *20*, 362.
(30) Leito, I.; Herodes, K.; Huopolainen, M.; Virro, K.; Kunnapas, A.; Kruve, A.; Tanner, R. *Rapid Commun. Mass Spectrom.* **2008**, *22*, 379.
(31) Di Marco, V. B.; Bombi, G. G. *Mass Spectrom. Rev.* **2006**, *25*, 347.
(32) As Figure S1 reveals, the initial dissolution process (reaction 1, Scheme 1) is not adequately represented in the fractional presentation. When no L^3 has been introduced to the solution, $[Au(PPh_3)_2]^+$ does constitute 100% of the ions in solution, but the total number of ions increases significantly as soon as some L^3 is added. It is possible that the process whereby complementary ions are formed is promoted by the introduction of some L^3. The data does not imply that L^3 must coordinate to each individual Au center in order to promote dissolution to ions, but suggests that if L^3 displaces one PPh_3 or Cl, excess PPh_3 or Cl becomes available in solution, promoting ligand exchange (even if the ligands merely become labile, exchanging with other identical ligands). Prior to the availability of excess ligands in solution, there is no strong driving force for dissolution to ions.
(33) Wang, J. C. *Acta Crystallogr. Sect. C-Cryst. Struct. Commun.* **1996**, *52*, 611.
(34) Atkins, P. W. *Physical Chemistry*; Oxford University Press: Oxford, 1978.
(35) See, for example:(a) Atwood, J. D.; Wovkulich, M. J.; Sonnenberger, D. C. *Acc. Chem. Res.* **1983**, *16*, 350. (b) Darensbourg, D. J.; Zalewski, D. J.; Delord, T. *Organometallics* **1984**, *3*, 1210.

JP804046E